Fully self-consistent calculations of momentum distributions of annihilating electron-positron pairs in SiC

Julia Wiktor, Gérald Jomard, Marc Torrent, Marie-France Barthe, M. Bertolus

Fully self-consistent calculations of momentum distributions of annihilating electron-positron pairs in SiC

Julia Wiktor,[1,*] Gérald Jomard,[1] Marc Torrent,[2] Marie-France Barthe,[3] and Marjorie Bertolus[1]
[1]*Commissariat à l'Energie Atomique, DEN, DEC, Centre de Cadarache, 13108 Saint-Paul-lez-Durance, France*
[2]*Commissariat à l'Energie Atomique, DAM, DIF, F-91297 Arpajon, France*
[3]*Centre National de la Recherche Scientifique, UPR 3079, CEMHTI, 45071 Orléans, France*
(Received 14 February 2016; published 13 May 2016)

We performed calculations of momentum distributions of annihilating electron-positron pairs in various fully relaxed vacancy defects in SiC. We used self-consistent two-component density functional theory schemes to find the electronic and positronic densities and wave functions in the considered systems. Using the one-dimensional momentum distributions (Doppler-broadened annihilation radiation line shapes) we calculated the line-shape parameters S and W. We emphasize the effect of the experimental resolution and the choice of the integration ranges for the S and W parameters on the distributions of the points corresponding to different defects in the $S(W)$ plot. We performed calculation for two polytypes of SiC, $3C$, and $6H$ and showed that for silicon vacancies and clusters containing this defect there were no significant differences between the Doppler spectra. The results of the Doppler spectra calculations were compared with experimental data obtained for n-type $6H$-SiC samples irradiated with 4-MeV Au ions. We observed a good general agreement between the measured and calculated points.

DOI: 10.1103/PhysRevB.93.195207

I. INTRODUCTION

Silicon carbide is a ceramic with a high melting point, a good chemical stability, and a low neutron absorption. These properties make it a possible cladding material in high-temperature fission reactors [1] and for the accident tolerant fuels in generation II and III reactors [2,3]. Additionally, its mechanical properties as a composite material make it an interesting material for fuel assembly envelopes [4].

During irradiation in a reactor the fission of actinide nuclei causes the creation of large amounts of defects, which affect the physical and chemical properties of materials inside the reactor, in particular fuel and structural materials. In the case of nuclear applications of silicon carbide, it is essential to understand the effects of the irradiation on its thermomechanical properties, for instance through defects creation and their interaction with fission products.

One of the nondestructive methods that can be used to characterize these defects is positron annihilation spectroscopy (PAS) [5,6]. There are two positron annihilation characteristics that allow one to detect defects in materials: the first one, the positron lifetime, is mostly sensitive to the open volume of defects. Second, the Doppler broadening of the annihilation radiation, carries information on the chemical environment in which positrons annihilate. However, positron annihilation spectroscopy results do not provide a direct link between the signal and the type of the defect. Therefore, the interpretation of experimental data often requires comparisons with other experimental techniques or with electronic structure calculations.

We have recently performed fully self-consistent calculations of positron lifetimes of monovacancies and vacancy clusters in SiC [7–9] and showed the importance of taking into account atomic relaxation effects on the identification of defects. We showed as well that in some cases various defects can exhibit similar positron lifetimes, leading to uncertainties in their identification in PAS experiments based on this characteristic only. In this work, we use our recent implementation [10] of the calculations of the momentum distributions of annihilating electron-positron pairs in the ABINIT code [11–14], to study defects in two polytypes of silicon carbide, $3C$ and $6H$-SiC.

This paper is organized as follows. In Sec. II we present the computational methods. In Sec. III we describe the calculated Doppler spectra and S and W parameters. We discuss the results and compare them with experiments in Sec. IV and conclude the paper in Sec. V.

II. METHODS

To perform the calculations of the momentum distributions of the annihilating electron-positron pairs we used the implementation of the two-component density functional theory [5,15,16] within the projector augmented-wave (PAW) [17–20] framework, available in the ABINIT [11–14] code. The computational methods are described in detail in Ref. [10] and here we recall them only briefly.

The present calculations of the momentum distributions of the annihilating electron-positron pairs are performed in the so-called "state-dependent" [21,22] scheme. This method has been chosen in the present study, since Makkonen *et al.* [23] showed that it yields better defect-to-bulk ratios of the Doppler spectra, that are usually considered in experimental studies, than the second available method—the state-independent scheme. The state-dependent momentum distribution $\rho(\mathbf{p})$ is expressed as

$$\rho(\mathbf{p}) = \pi r_e^2 c \sum_j \gamma_j \left| \int d\mathbf{r}\, e^{-i\mathbf{p}\cdot\mathbf{r}} \Psi^+(\mathbf{r}) \Psi_j^-(\mathbf{r}) \right|^2, \quad (1)$$

*Current address: Chaire de Simulation à l'Echelle Atomique, Ecole Polytechnique Fédérale de Lausanne, CH-1015 Lausanne, Switzerland.

where $\Psi^+(\mathbf{r})$ is the positron wave function, $\Psi_j^-(\mathbf{r})$ is the wave function of the electronic state j, $\mathbf{p}$ is a given momentum, r_e is the classical electron radius, and c is the speed of light. In the above equation γ_j is equal to $\lambda_j/\lambda_j^{\mathrm{IPM}}$, where λ_j is the total annihilation rate calculated for the electronic state j:

$$\lambda_j = \pi r_e^2 c \int d\mathbf{r}\, n_j^-(\mathbf{r}) n^+(\mathbf{r}) \gamma(n^-), \tag{2}$$

and λ_j^{IPM} is the annihilation rate calculated for the same state within the independent particle model, hence using $\gamma = 1$. $n^+(\mathbf{r})$ is the positron density and $n_j^-(\mathbf{r})$ is the density corresponding to the electron state j.

In this work we use the so-called conventional scheme to calculate Doppler spectra for the perfect lattice. In this case the local-density approximation (LDA) zero-positron density limit of the electron-positron correlation functional, parametrized by Boroński and Nieminen [16] using the data provided by Arponen and Pajanne [24], is used.

In momentum distribution calculations for vacancies, we apply a fully self-consistent scheme, using a full LDA electron-positron correlation functional provided by Puska, Seitsonen, and Nieminen [25] and an enhancement factor depending on both the electron and the positron densities, $g(n^-,n^+)$. In this case Eq. (2) becomes

$$\lambda_j = \pi r_e^2 c \int d\mathbf{r}\, n_j^-(\mathbf{r}) n^+(\mathbf{r}) g(n^-,n^+). \tag{3}$$

The self-consistent calculations are performed as a double loop on the electronic and positronic densities: during each subloop, one of the two densities is kept constant while the other is being converged. Additionally, we allow the atomic positions to relax, according to the electronic and positronic forces.

It is worth noting that besides the LDA parametrization of the electron-positron correlation functional and enhancement factor used here various other methods have been developed. For instance Stachowiak and Lach [26] suggested a LDA form of γ within the perturbed hypernetted-chain approximation and Drummond *et al.* [27] proposed new formulations of both the electron-positron correlation functional and the enhancement factor based on a fit to quantum Monte Carlo data. On top of various LDA parametrizations, generalized gradient approximation correction can be also applied, such as semiempirical ones by Barbiellini *et al.* [28,29] and Kuriplach and Barbiellini [30,31] or a recent parameter free gradient correction by Barbiellini and Kuriplach [32]. The above parametrizations exist only for the zero-positron density limit, therefore their use is mostly justified in the studies of delocalized positrons in perfect materials. Since this study is dedicated to defects, we decide to use the full LDA electron-positron correlation functional by Puska, Seitsonen, and Nieminen with the corresponding Boroński and Nieminen parametrization for delocalized positrons. We do not apply the gradient corrections, since it was shown by Makkonen *et al.* [23] that even though this method yields absolute Doppler spectra in better agreement with experiments the better relative ratios are obtained using the LDA scheme of Boroński and Nieminen.

Both the electronic and positronic wave function are described using the same mixed basis (plane waves and atomic orbitals) in the framework of the PAW method. The PAW data sets were generated using a modified version of the ATOMPAW code [19]. For carbon we included six electrons ($1s$, $2s$, and $2p$) and for silicon four electrons ($3s$ and $3p$) in the valence state. Additionally, to achieve a correct description of the positron wave function, we added $2s$ and $2p$ states in the Si basis set (see Ref. [10] for discussion on the PAW data set completeness for the positron description).

Calculations for defects are performed using 216 and 192 atom supercells for $3C$-SiC and $6H$-SiC, respectively. We use LDA for the electron-electron exchange-correlation functional. For both polytypes we use theoretical lattice parameters yielded by this approximation, $a = b = c = 4.33$ Å for $3C$-SiC and $a = b = 3.06$ Å and $c = 15.03$ Å for $6H$-SiC. To study negatively charged defects we use supercells including additional electrons. In these cases, a compensating background charge is introduced to restore the global charge neutrality (for more details on the treatment of charged cells in the PAW framework in ABINIT see Ref. [33]). The positron wave function and density are calculated at two $\mathbf{k}$ points, the Γ point and another one chosen to lie on the edge of the Brillouin zone, to avoid the delocalization of the positron due to the small supercell, as proposed by Korhonen *et al.* [34]. The same $\mathbf{k}$ points are used in the electronic calculations. The momentum distributions have been calculated using the wave functions corresponding to the Γ point only. We used the cutoff energy of 680 eV, since we found it was enough to obtain Doppler spectra converged up to 40 mrad.

All defects considered in this study are allowed to relax. The atomic relaxations are performed until the forces acting on atoms become smaller than 0.03 eV/Å. In some cases we start the relaxation from the ideal geometry, while in the others from the geometry of a defect without the positron. We find that the starting point does not influence the final result, nor the total computation time. In the following, we always discuss the relaxation relative to the ideal geometries.

For comparison with experiments we calculate one-dimensional projections (Doppler spectra) of the three-dimensional momentum densities in three different directions. This is done by integrating the momentum distribution along the two remaining directions, using the expression as follows:

$$\rho(p_z) = \iint dp_x\, dp_y\, \rho(\mathbf{r}). \tag{4}$$

In experiments, directions cannot usually be distinguished. Therefore, we calculate projections in three different directions and average the results. To obtain the best quality Doppler spectra, we choose p_z to be normal to the dense (001), (011), and (111) planes. In the cubic $3C$-SiC it is equivalent to [001], [011], and [111] directions and in $6H$-SiC it is equivalent to [001], $[\frac{a}{2}\ \frac{a\sqrt{3}}{2}\ c]$, and $[a\ 0\ c]$ directions, where a and c are the lattice parameters of this structure.

Additionally, to mimic the finite resolution of experimental measurements we convolve the theoretical results with a Gaussian function with a full width at half maximum (FWHM) close to the experimental resolution. We further interpolate the one-dimensional spectra on a grid with 0.1-mrad spacing and normalize the spectra to unity.

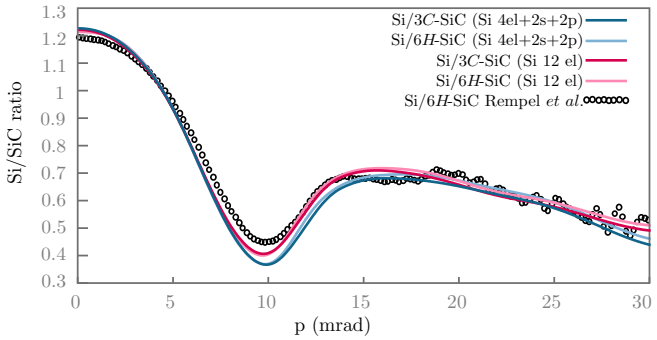

FIG. 1. Si lattice/SiC lattice ratio curves of momentum distribution of annihilation radiation. The theoretical results obtained using different silicon PAW data sets are compared with experimental data obtained by Rempel *et al.* [35]. The theoretical curves are convoluted with a Gaussian function with a FWHM of 3.6 mrad.

III. RESULTS

A. Perfect lattice

We first performed momentum distribution calculations for the perfect lattice of SiC. To be able to make a comparison with the experimental data of Rempel *et al.* [35] for 6*H*-SiC, in Fig. 1 we present the result as ratios of Si lattice to SiC lattice. For Si we used two different PAW data sets: one with 12 valence electrons and one with four valence electrons and additional 2*s* and 2*p* states in the basis set. For carbon, we use a data set including all six electrons in the valence state. The results calculated using both PAW data sets are in very good agreement with the experimental data. In the figure we present the results obtained for both 3*C*-SiC and 6*H*-SiC. It can be seen that the momentum distributions of the silicon carbide lattice are very similar for the two polytypes.

B. Defects relaxation

For all defects considered here we observe an outward relaxation due to the positron localization, both in respect to the ideal geometries and geometries of defects without the positron (see Refs. [7,9] for details and final geometries of the defects). In general, we do not observe any important modifications in the defects symmetries, except for the carbon monovacancy, in which case the defect itself relaxes inwards in a D_{2d} geometry, while the positron breaks the bonds between silicon atoms and induces an outward relaxation in a T_d geometry [7]. Figure 9 in Ref. [10] illustrates the influence of the outward relaxation of the defect on the momentum distribution for the silicon vacancy in Si. Larger volume of a vacancy leads to a stronger localization of the positron. At the same time the annihilation rate increases for the valence electrons and decreases for the core states.

C. Neutral vacancies in 3*C*-SiC

Figure 2 shows the results obtained for fully relaxed neutral vacancies in 3*C*-SiC as ratios to perfect lattice. All the spectra presented in this section have been convolved with a Gaussian function with FWHM = 4.7 mrad, which corresponds to the resolution of many experimental studies performed on

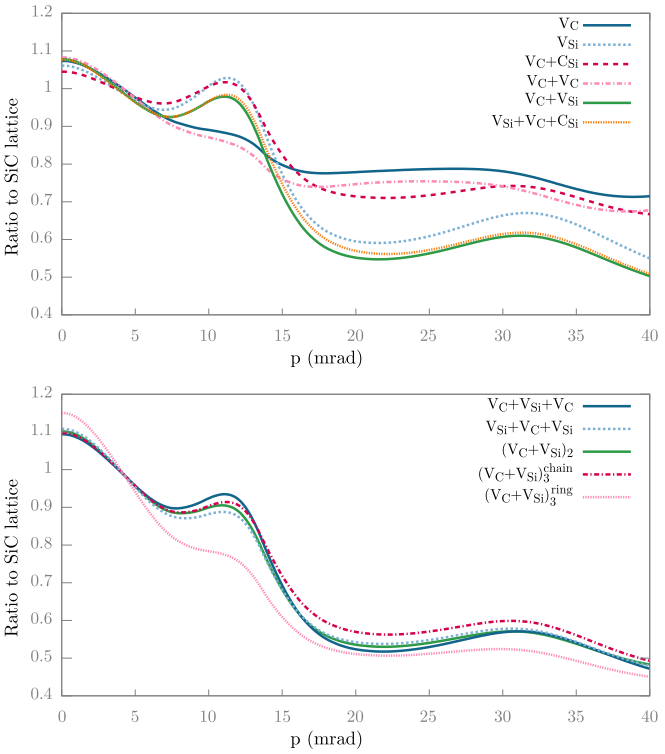

FIG. 2. Ratio curves of the calculated momentum distributions of annihilating electron-positron pairs in various vacancies in SiC. All spectra are convoluted with a Gaussian of 4.7 mrad and divided by the lattice spectrum.

SiC. The results are shown for momenta between 0 and 40 mrad, which are the ranges usually used when presenting experimental data.

We can observe a clear difference between the shapes of the ratio curves obtained for monovacancies on the C and Si sublattices. The ratio calculated for the carbon vacancy has a maximum of around 1.07 at $p = 0$, decreases below 1 for momenta higher that 4 mrad, and exhibits two slight shoulders, one at 11.5 mrad and one around 30 mrad. The form of the ratio calculated for the $V_C + V_C$ divacancy is very similar to that of V_C, the latter being slightly closer to the perfect lattice.

For V_{Si} we also observe a maximum of around 1.06 at $p = 0$ and the ratio curve drops below 1 at around 4 mrad. Contrary to V_C, a peak can be observed at around 11.5 mrad, with a value above 1. This peak could be attributed to the annihilation with 2*p* electrons of the carbon atoms, which are expected to be the ones most likely to annihilate with the positron localized at the silicon site. Another peak is observed above 30 mrad with a value around 0.67. The overall shape of the ratio calculated for V_{Si} is in agreement with the previous calculations for this defect performed by Kawasuso *et al.* [36], even if the high-momentum ratio is slightly lower in our calculations (with differences around 0.1). This could be due to the atomic relaxation, which was not fully taken into account in the study of Kawasuso *et al.* (calculations were performed using relaxed geometries of empty defects, therefore the effect of positronic forces was neglected). Our result at high momenta can be also compared to calculations by Barbiellini *et al.* [37] who studied the core contributions of the

positron-electron momentum distributions for monovacancies and the $V_C + V_{Si}$ divacancy in 3*C*-SiC. They observed a 57% decrease of the core contribution for V_{Si}, as compared to the perfect lattice, while in our calculations this value is between 40 and 50% at momenta close to 40 mrad.

The ratio curve calculated for the $V_C + C_{Si}$ cluster has a shape similar to that of the silicon vacancy at low momenta. This can be explained by the fact that even though in this defect the positron is surrounded by one carbon and three silicon atoms it localizes closer to the antisite C atom (see Fig. 8 in Ref. [9]) and the annihilation rate should be the highest with its electrons. The ratio calculated for $V_C + C_{Si}$ is significantly higher at $p > 15$ mrad than the one for V_{Si}, since the volume of the former defect is smaller. This leads to a larger annihilation rate with core electrons.

The ratio curve calculated for the $V_C + V_{Si}$ divacancy has a similar shape to that found for the silicon vacancy. However, since the divacancy has a larger open volume, we observe a higher contribution at the low momenta and a decreased annihilation rate with more energetic electrons. The $V_C + V_{Si}$ divacancy was also studied by Barbiellini *et al.* [37]. At high momenta (around 40 mrad) they find the ratio of around 0.53, close to our value of around 0.5.

As far as larger clusters are concerned, similar ratio curves are found for the $V_C + V_{Si} + V_C$, $V_{Si} + V_C + V_{Si}$, $(V_C + V_{Si})_2$, and $(V_C + V_{Si})_3^{chain}$ defects. The result found for the $(V_C + V_{Si})_3^{ring}$ hexavacancy can be, however, easily distinguished from the other ones. In this case the value at $p = 0$ is much higher, due to a larger open volume of this defect, and the peak around $p = 11.5$ mrad transforms into a shoulder. It is interesting to notice that the ratio curve of $(V_C + V_{Si})_3^{ring}$ has a form which is more similar to that of V_C than to that of V_{Si}, especially at low momenta. It is probably due to the fact that this defect has a large three-dimensional volume and the localized positron interacts mostly with the Si valence electrons and not with the more localized C electrons.

D. *S* and *W* parameters: Effect of the experimental resolution and integration windows

For the interpretation of the experimental studies the *S* and *W* parameters are usually analyzed instead of the ratio curves. We therefore calculated these parameters for the considered defects. In the following sections we will discuss the relative parameters, calculated as

$$S_{rel} = \frac{S_{defect}}{S_{lattice}} \quad \text{and} \quad W_{rel} = \frac{W_{defect}}{W_{lattice}}. \tag{5}$$

In the case of *S* and *W* it is important to stress the importance of the resolution and of the choice of the windows in which these parameters are calculated on the results. In Fig. 3 we present the S_{rel} parameter as a function of the W_{rel} parameter plotted for various neutral defects in 3*C*-SiC using spectra convoluted with Gaussian functions with various FWHM. We chose two cases corresponding to the experimental measurements using either two Ge detectors in coincidence mode (FWHM = 3.6 mrad) or a single Ge detector (FWHM = 4.7 mrad). These parameters are calculated using windows of 0–2.86 and 10.58–27.36 mrad for *S* and *W*, respectively. We can observe that the results obtained using the higher FWHM are shifted towards the point corresponding to the lattice, (1,1), but the relative positions of the points corresponding to each defect on the plot are conserved for the two resolutions.

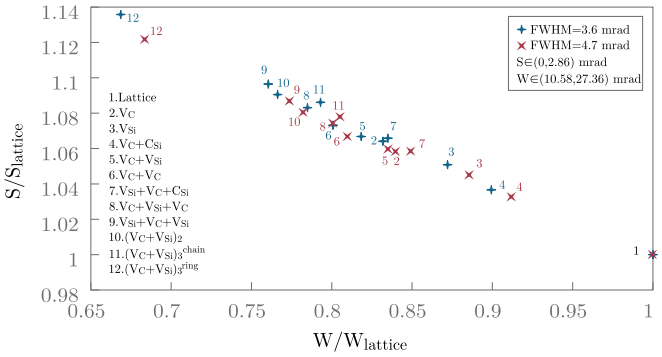

FIG. 3. S_{rel} parameter as a function of the W_{rel} parameter plotted for various neutral defects in 3*C*-SiC using spectra convoluted with Gaussian functions with different FWHM. The parameters are calculated using windows (0,2.86) and (10.58,27.36) mrad for *S* and *W*, respectively.

The effect of the choice of the windows in which the *S* and *W* parameters are integrated is presented in Fig. 4. In this case we plotted the results using two sets of windows, $S \in (0,2.5)$ mrad and $W \in (15.0,27.36)$ mrad on the one hand and $S \in (0,2.86)$ mrad and $W \in (10.58,27.36)$ mrad on the other hand. We observe that the results are much more sensitive to the the high-momentum window than to the low-momentum one. It is interesting to see that when the first set of windows is used the points are easier to distinguish. In particular, the points corresponding to defects on the carbon sublattice (V_C and $V_C + V_C$) are well separated from the other ones. When the second set of windows is used, all points are almost exactly aligned on the line passing through the (1,1) point. It means that the choice of the ranges within which the *W* is calculated can help to distinguish defects in experiments. Another consequence of the high sensitivity of the *W* parameter to the integration range choice is that the comparison between published data can be difficult, since different windows are usually used for each study.

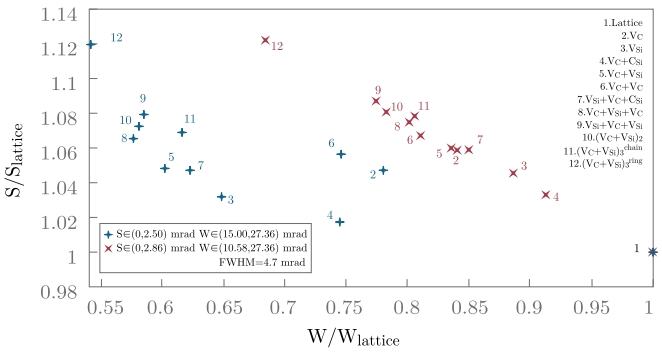

FIG. 4. S_{rel} parameter as a function of the W_{rel} parameter plotted for various neutral defects in 3*C*-SiC using different windows for *S* and *W* parameters. The results were obtained using spectra convoluted with a Gaussian function with FWHM = 4.7 mrad.

TABLE I. Relative S_{rel} and W_{rel} parameters calculated for various defects in 3C-SiC, using different resolutions and integration.

	FWHM = 3.6 mrad $S \in (0,2.86)$ mrad $W \in (10.58,27.36)$ mrad		FWHM = 4.7 mrad $S \in (0,2.86)$ mrad $W \in (10.58,27.36)$ mrad		FWHM = 4.7 mrad $S \in (0,2.5)$ mrad $W \in (15,27.36)$ mrad	
Defect	S_{rel}	W_{rel}	S_{rel}	W_{rel}	S_{rel}	W_{rel}
V_C	1.064	0.832	1.058	0.840	1.060	0.780
V_{Si}	1.051	0.871	1.045	0.886	1.048	0.648
$V_C + C_{Si}$	1.037	0.900	1.033	0.912	1.035	0.744
$V_C + V_C$	1.073	0.801	1.066	0.810	1.069	0.745
$V_C + V_{Si}$	1.067	0.818	1.060	0.835	1.063	0.601
$V_{Si} + V_C + C_{Si}$	1.066	0.835	1.058	0.849	1.061	0.622
$V_C + V_{Si} + V_C$	1.083	0.785	1.074	0.801	1.078	0.575
$V_{Si} + V_C + V_{Si}$	1.097	0.760	1.087	0.774	1.091	0.585
$(V_C + V_{Si})_2$	1.090	0.766	1.081	0.782	1.085	0.580
$(V_C + V_{Si})_3^{chain}$	1.087	0.792	1.078	0.804	1.081	0.651
$(V_C + V_{Si})_3^{ring}$	1.135	0.669	1.122	0.684	1.127	0.541

The S_{rel} and W_{rel} parameters calculated using various resolutions and integration windows, which were used to generate Figs. 3 and 4, are also presented in Table I for all the considered defects.

E. Effect of the charge state

We verified the effect of the charge state on the momentum distribution by performing calculations on V_{Si} in 3C-SiC. We calculated the ratio curves for this defect for 0, −1, and −2 charge states. The results are presented in Fig. 5. We can observe that the ratio at $p = 0$ decreases when the negative charge increases. It is due to the fact that the relaxation for the negative vacancies is smaller than for the neutral ones [7]. This is reflected in the corresponding S_{rel} [$S \in (0,2.86)$ mrad] as shown in Table II. The peak close to $p = 10$ mrad rises when electrons are added to the system, while at the same time the ratio at momenta higher than approximately 17 mrad decreases. Both regions are included in the window used to calculate the W parameter, 10.58–27.36 mrad, however their effects do not cancel each other out and we can observe an increase in W due to the additional negative charge.

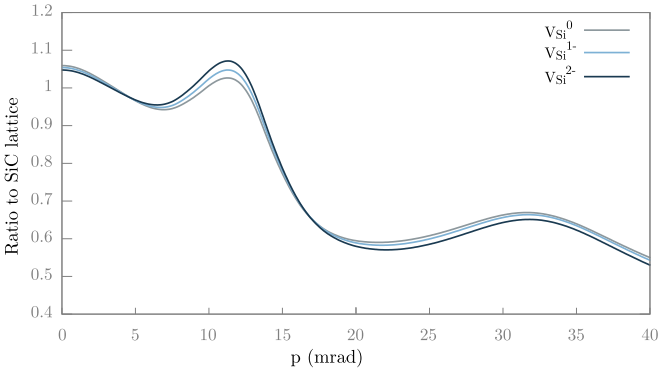

FIG. 5. Ratio curves of the calculated momentum distributions of annihilating electron-positron pairs in neutral and charged silicon vacancy in 3C-SiC. All spectra are convoluted with a Gaussian function with FWHM = 4.7 mrad and divided by the lattice spectrum.

F. Comparison of 3C and 6H polytypes

In Sec. III A, we showed that there was no significant difference between the perfect 3C and 6H lattices. The comparison must also be performed for vacancies. In Figs. 6–9 we present the ratio curves obtained for V_C, $V_C + C_{Si}$, V_{Si}, and $V_C + V_{Si}$ defects in two polytypes of silicon carbide. Table III shows the relative S and W parameters calculated for these defects.

In the case of the carbon vacancy (Fig. 6) in 6H-SiC we observe a strong dependence of the ratio curve on the site. The result obtained for the h site is quite similar to that calculated in the 3C polytype. For k_1 and k_2 the ratio curves are flatter. It is consistent with what was observed in the calculations of positron lifetimes, where a smaller outward relaxation and hence a weaker localization of the positron was observed for the cubic sites. It is also reflected in the S_{rel} and W_{rel} parameters which are closer to 1 for k_1 and k_2 (see Table III).

The dependence of the calculated ratio on the local geometry is lower for the $V_C + C_{Si}$ complex (Fig. 7), but it can still be observed. The positron localization is the strongest in the 3C polytype and in the $h - h$ configuration in 6H-SiC. As was already observed in the results of the positron lifetimes calculations, the weakest relaxation is found for the $k_2 - k_2$ configuration [9]. This is reflected in smaller low- and larger high-momentum contributions.

As for the defects in which the positron is localized mostly inside the silicon vacancy, V_{Si} and $V_C + V_{Si}$, the ratio curves are very similar (see Figs. 8 and 9). The differences are easier to observe in S_{rel} and W_{rel} parameters (see Table III). However,

TABLE II. Relative S_{rel} and W_{rel} parameters calculated for various charge states of V_{Si}. The parameters were obtained using windows of 0–2.86 and 10.58–27.36 mrad for S and W, respectively. The spectra were convoluted with a Gaussian function with FWHM = 4.7 mrad.

	S_{rel}	W_{rel}
V_{Si}^{0}	1.045	0.886
V_{Si}^{1-}	1.040	0.899
V_{Si}^{2-}	1.035	0.913

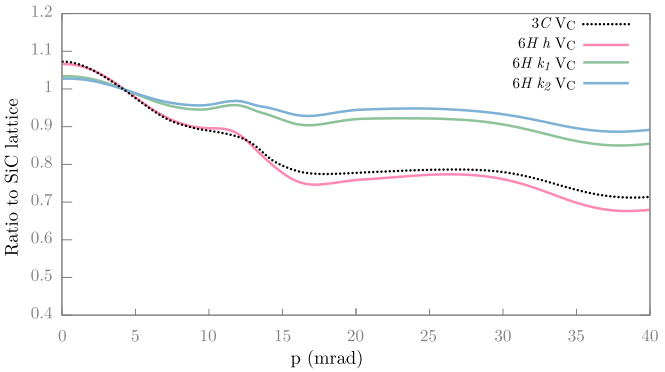

FIG. 6. Ratio curves of the calculated momentum distributions of annihilating electron-positron pairs in V_C in 3C and 6H polytypes of silicon carbide. All spectra are convoluted with a Gaussian function with FWHM = 4.7 mrad and divided by the lattice spectrum.

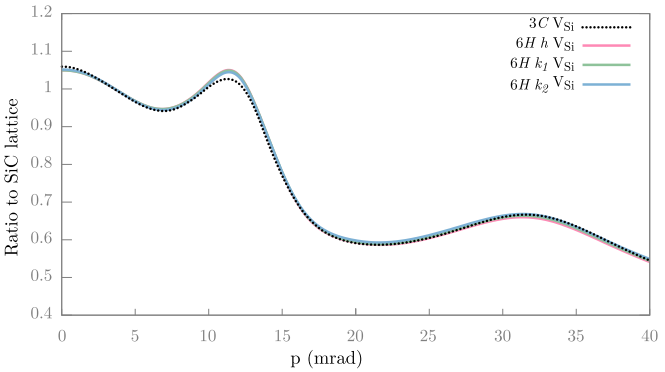

FIG. 8. Ratio curves of the calculated momentum distributions of annihilating electron-positron pairs in V_{Si} in 3C and 6H polytypes of silicon carbide. All spectra are convoluted with a Gaussian function with FWHM = 4.7 mrad and divided by the lattice spectrum.

we consider that these differences are probably much lower than the experimental precision, hence not significant when it comes to defect identification.

Based on the small differences between the two polytypes obtained for V_{Si} and $V_C + V_{Si}$, similarly to what was observed in the positron lifetime calculations, we conclude that the Doppler broadening calculations performed for clusters in 3C-SiC can also be used to analyze experimental data obtained for other polytypes.

G. Effect of the nitrogen decoration of vacancies

In the majority of experimental studies on SiC discussed in this work, n-type samples were studies. In this case, the material is doped with nitrogen (with concentrations above 10^{17} cm^{-3}), which usually substitutes the carbon sites and can form complexes with vacancies. We studied the effect of the nitrogen decoration of silicon vacancies on the Doppler spectra and the S and W parameters. The calculated ratio curves are shown in Fig. 10. In Fig. 11 we present the S_{rel} and W_{rel} parameters, calculated using two sets of integration windows, $S \in (0,2.5)$ mrad and $W \in (15.0,27.36)$ mrad on the one hand and $S \in (0,2.86)$ mrad and $W \in (10.58,27.36)$ mrad on the other hand. In Fig. 10 we can observe that adding nitrogen atoms next to the silicon monovacancy leads to the decrease of the peak at $p = 0$ and to the increase of the ratio curve above around $p = 5$ mrad. The changes in the curve seem to be proportional to the number of nitrogen atoms surrounding the silicon vacancy.

As for the $S(W)$ plot (Fig. 11) we can observe that the decoration of the silicon monovacancy with nitrogen atoms leads to a clear shift of the corresponding points from the line connecting the lattice and V_{Si}. Moreover, the direction of that shift depends on the chosen integration windows. For $S \in (0,2.5)$ mrad and $W \in (15.0,27.36)$ mrad the points corresponding to the complexes with nitrogen are on the left side of the line, while for $S \in (0,2.86)$ mrad and $W \in (10.58,27.36)$ mrad the points are on its right side.

IV. DISCUSSION AND COMPARISON WITH EXPERIMENTS

In this section we compare the Doppler spectra calculated for defects in silicon carbide with the experimental data

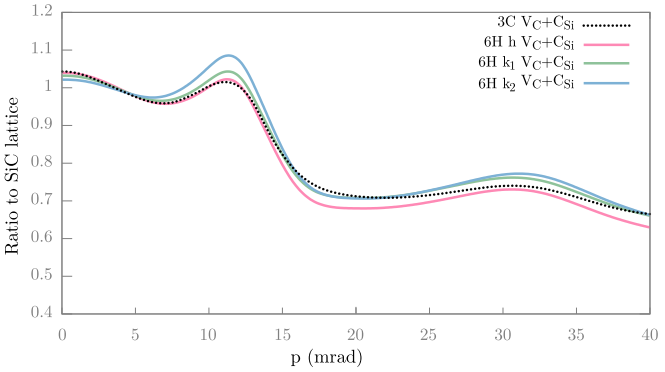

FIG. 7. Ratio curves of the calculated momentum distributions of annihilating electron-positron pairs in $V_C + C_{Si}$ complexes in 3C and 6H polytypes of silicon carbide. All spectra are convoluted with a Gaussian function with FWHM = 4.7 mrad and divided by the lattice spectrum.

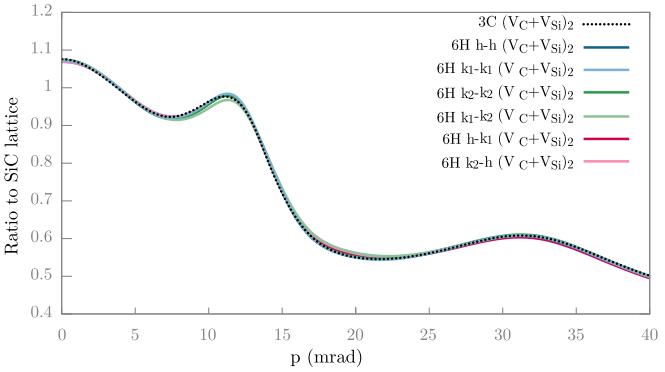

FIG. 9. Ratio curves of the calculated momentum distributions of annihilating electron-positron pairs in $V_C + V_{Si}$ complexes in 3C and 6H polytypes of silicon carbide. All spectra are convoluted with a Gaussian function with FWHM = 4.7 mrad and divided by the lattice spectrum.

TABLE III. Relative S_{rel} and W_{rel} parameters calculated for various defects in 3C and 6H silicon carbide. The parameters were obtained using windows of 0–2.86 and 10.58–27.36 mrad for S and W, respectively. The spectra were convoluted with a Gaussian function with FWHM = 4.7 mrad.

Defect	Site	S_{rel}	W_{rel}
V_C	3C	1.058	0.840
V_C	6H, h	1.056	0.836
V_C	6H, k_1	1.029	0.938
V_C	6H, k_2	1.024	0.954
V_{Si}	3C	1.045	0.886
V_{Si}	6H, h	1.040	0.901
V_{Si}	6H, k_1	1.040	0.901
V_{Si}	6H, k_2	1.041	0.900
$V_C + C_{Si}$	3C	1.032	0.912
$V_C + C_{Si}$	6H, $h - h$	1.033	0.903
$V_C + C_{Si}$	6H, $k_1 - k_1$	1.026	0.927
$V_C + C_{Si}$	6H, $k_2 - k_2$	1.017	0.955
$V_C + V_{Si}$	3C	1.060	0.835
$V_C + V_{Si}$	6H, $h - h$	1.063	0.839
$V_C + V_{Si}$	6H, $k_1 - k_1$	1.059	0.842
$V_C + V_{Si}$	6H, $k_2 - k_2$	1.061	0.840
$V_C + V_{Si}$	6H, $k_1 - k_2$	1.062	0.837
$V_C + V_{Si}$	6H, $h - k_1$	1.058	0.840
$V_C + V_{Si}$	6H, $k_2 - h$	1.057	0.841

obtained during the PhD thesis of Linez [38]. In this work n-type 6H-SiC samples were irradiated with 4-MeV Au ions with fluences from 10^{12} to 10^{15} cm^{-2}. These irradiations led to the creation of vacancies and vacancy clusters with various sizes. The samples were studied with two different low-energy positron beams, one allowing for Doppler measurements (continuous beam) and one allowing for measurements of positron lifetime (pulsed beam), with varying energies.

In Table IV we recall the positron lifetimes that were detected in the study of Linez in the cascade region of the irradiated SiC samples. In Fig. 12 we compare the measured and calculated S_{rel} and W_{rel} parameters. The calculated spectra were convoluted using a Gaussian function with FWHM = 4.7 mrad, which should be close to the experimental resolution in the reference study. We observe that the calculated points are slightly below the experimental points. However, an overall good agreement is obtained in the evolution trends of the relative S_{rel} and W_{rel} values. The differences can be due to the various approximations made in the calculations and to experimental uncertainties.

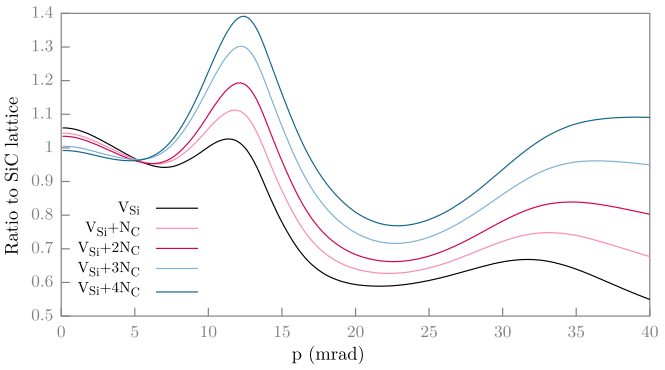

FIG. 10. Ratio curves of the calculated momentum distributions of annihilating electron-positron pairs in nitrogen-decorated silicon monovacancies in 3C-SiC. All spectra are convoluted with a Gaussian function with FWHM = 4.7 mrad and divided by the lattice spectrum.

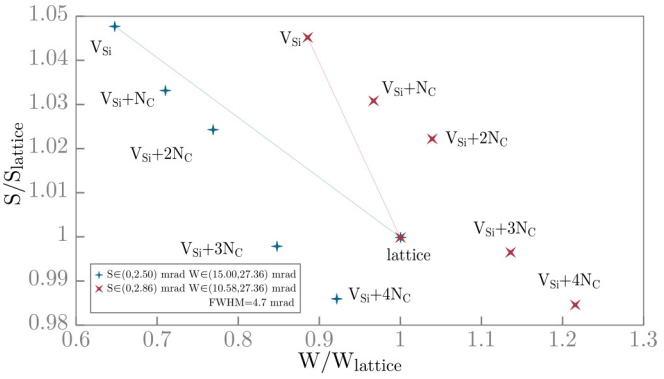

FIG. 11. S_{rel} parameter as a function of the W_{rel} parameter plotted for nitrogen-decorated silicon monovacancies calculated using two sets of integration windows. The results were obtained using spectra convoluted with a Gaussian function with FWHM = 4.7 mrad.

The experimental S_{rel} and W_{rel} parameters measured after irradiation at 10^{12} and 10^{13} cm^{-2} fluences do not align with any of the calculated values. However, they lay near the points calculated for V_{Si} and $V_{Si} + V_C + C_{Si}$. A long positron lifetime of 223–225 ps was measured after these irradiations, which is close to what was calculated for the silicon monovacancy. We suppose, hence, that a defect of a similar size was detected in these samples. It is worth noting that the experimental points measured after irradiation at 10^{12} and 10^{13} cm^{-2} fluences are above the line going through the (1,1) point and the data corresponding to samples irradiated at higher fluences (see dashed lines in Fig. 12). Meanwhile, for all the considered "pure" defects in silicon carbide we calculated points that are aligned on the line going through the (1,1) point. We can suppose, hence, that the shift of the experimental points can be due to the presence of impurities. In Fig. 11 we show that the nitrogen decoration of the silicon monovacancy leads to a similar shift of the points on the $S(W)$ plot. We suppose hence that after irradiation at 10^{12} and 10^{13} cm^{-2} fluences vacancy complexes with impurities, such as nitrogen, are detected. This effect cannot be observed at higher fluences, where large clusters dominate.

TABLE IV. Experimental positron lifetimes detected in 4-MeV Au irradiated 6H-SiC. Data were extracted from Ref. [38] In the case of the irradiation at 10^{14} cm^{-2} the positron lifetime varied as a function of the incident positron energy (between 5 and 11 keV).

Fluence (cm^{-2})	τ_1 (ps)	I_1 (%)	τ_2 (ps)	I_2 (%)
10^{12}	177 ± 0	6 ± 0.7	225 ± 0	94 ± 0.7
10^{13}	223 ± 1	100		
10^{14}	239 ± 0	96↘56	289 ± 0	4 ↗44
10^{15}	284 ± 1	100		

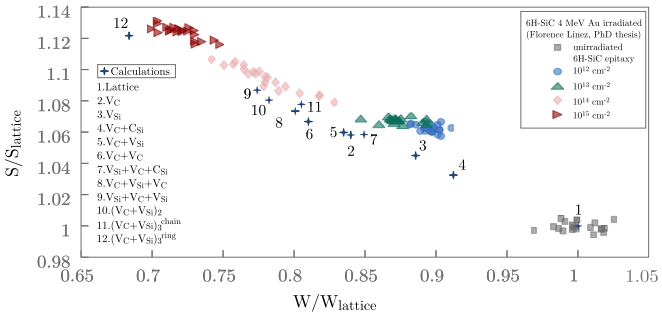

FIG. 12. Comparison between the calculated and experimental S_{rel} and W_{rel} parameters detected by Linez [38] in 4-MeV Au irradiated n-type 6H-SiC. The theoretical data were convoluted with a Gaussian function with FWHM = 4.7 mrad.

After irradiation at 10^{14} cm^{-2} fluence S_{rel} increases and W_{rel} decreases, compared to the values at lower fluences. The experimental points corresponding to this irradiation are distributed along a line starting above the point calculated for $V_C + V_{Si}$ and going in the direction of the $(V_C + V_{Si})_3^{ring}$ complex. Several other complexes can correspond to the experimental points, $V_C + V_C$, $V_C + V_{Si} + V_C$, $V_{Si} + V_C + V_{Si}$, $(V_C + V_{Si})_2$, and $(V_C + V_{Si})_3^{chain}$. The positron lifetimes measured in this sample vary from 239 to 289 ps when the incident positron energy increases, which corresponds to increasing depths probed by the positrons. It means that defects of different sizes, probably between divacancies and hexavacancies, were created in this sample. However, in the region of the $S_{rel}(W_{rel})$ plot corresponding to the irradiation at 10^{14} cm^{-2} fluence, various theoretical points are close to each other and difficult to distinguish. It could be useful to have access to whole experimental ratio curves or to recalculate the experimental parameters using a different high-momentum integration region, since this can help in separating some of the points on the $S_{rel}(W_{rel})$ plot, as was shown in Fig. 4.

After irradiation at the 10^{15} cm^{-2} fluence the experimental points move further towards the point calculated for the $(V_C + V_{Si})_3^{ring}$ cluster. The measured S_{rel} and W_{rel} parameters are close to the value calculated for the "ring" hexavacancy, but slightly shifted towards the points calculated for smaller defects. We suppose that several defects are detected at the same time, while $(V_C + V_{Si})_3^{ring}$ is predominant. This is consistent with the positron lifetime measured in this sample. The value of around 284 ps is lower than what we calculated for $(V_C + V_{Si})_3^{ring}$ (296 ps when scaled to the experimental lattice lifetime), suggesting that some defects with smaller free volumes are also present in the sample.

Combining the information on the positron lifetimes and Doppler spectra can facilitate the defects identification. We can see, however, that in some cases it is still difficult to distinguish the defects. It would hence be useful to confirm our conclusions by coupling positron lifetime and Doppler broadening measurements with another experimental technique, for instance photoluminescence spectroscopy, performed on the same samples. Moreover, we observe that when comparing experimental and calculated momentum distributions general trends and evolutions should be considered and not absolute values. It most likely means that a different choice of the electron-positron correlation functional or enhancement factor (see Sec. II for various existing parametrizations) would lead to similar conclusions.

V. CONCLUSIONS

We performed self-consistent calculations of the momentum distributions of annihilating electron-positron pairs in various fully relaxed vacancy defects in two polytypes of SiC, 3C, and 6H. We observed that for the perfect lattice and defects containing silicon vacancies similar results were found in the two structures. The largest differences were found for the carbon vacancy, mostly due to smaller atomic relaxation at the k_1 and k_2 sites in 6H-SiC for this defect. We also studied the effect of the charge state and nitrogen decoration on the calculated spectra and S and W parameters.

We studied the effect of the experimental parameters on the S and W parameters that are commonly used to analyze the results. We showed the effect of the experimental resolution and the integration windows on the calculated S and W. We observed that an appropriate choice of the high-momentum integration region can facilitate the separation of the defects, especially on different sublattices.

The results of the Doppler spectra calculations were compared with experimental data. We observed a good general agreement between the measured and calculated points. However, it was shown that due to the choice of the integration windows in S and W parameters calculations the points corresponding to different defects are aligned and difficult to distinguish, even when coupling the results with the information on positron lifetimes. We concluded that it could be useful to recalculate the experimental parameters using a different high-momentum integration region and to couple the positron lifetime and Doppler broadening measurements with another type of experiment, for instance photoluminescence spectroscopy, performed on the same samples.

ACKNOWLEDGMENTS

This work was partly performed using high-performance computing resources from Le Centre de calcul recherche et technologie of the Grand équipement national de calcul intensif (GENCI-CCRT) (Grant No. x2015096008) and was supported by the French program Nucléaire, Energie, Environnement, Déchets et Société (NEEDS).

[1] P. Yvon and F. Carré, J. Nucl. Mater. **385**, 217 (2009).
[2] H. Feinroth, M. Ales, E. Barringer, G. Kohse, D. Carpenter, and R. Jaramillo, in *Ceramics in Nuclear Applications*, edited by Y. Katoh, A. Cozzi, D. Singh, and J. Salem (John Wiley & Sons, Inc., Hoboken, NJ, USA, 2009).
[3] H. Feinroth, E-Journal of Advanced Maintenance **5**, 128 (2013).
[4] N. P. Bansal and J. Lamon, *Ceramic Matrix Composites: Materials, Modeling and Technology* (Wiley, New York, 2014).
[5] M. J. Puska and R. M. Nieminen, Rev. Mod. Phys. **66**, 841 (1994).

[6] F. Tuomisto and I. Makkonen, Rev. Mod. Phys. **85**, 1583 (2013).
[7] J. Wiktor, G. Jomard, M. Torrent, and M. Bertolus, Phys. Rev. B **87**, 235207 (2013).
[8] J. Wiktor, G. Jomard, and M. Bertolus, Nucl. Instrum. Methods B **327**, 63 (2014).
[9] J. Wiktor, X. Kerbiriou, G. Jomard, S. Esnouf, M.-F. Barthe, and M. Bertolus, Phys. Rev. B **89**, 155203 (2014).
[10] J. Wiktor, G. Jomard, and M. Torrent, Phys. Rev. B **92**, 125113 (2015).
[11] X. Gonze, G.-M. Rignanese, M. Verstraete, J.-M. Beuke, Y. Pouillon, R. Caracas, F. Jollet, M. Torrent, G. Zérah, M. Mikami *et al.*, Z. Kristallogr. **220**, 558 (2005).
[12] X. Gonze, J.-M. Beuken, R. Caracas, F. Detraux, M. Fuchs, G.-M. Rignanese, L. Sindic, M. Verstraete, G. Zérah, F. Jollet *et al.*, Comput. Mater. Sci. **25**, 478 (2002).
[13] X. Gonze, B. Amadon, P.-M. Anglade, J.-M. Beuken, F. Bottin, P. Boulanger, F. Bruneval, D. Caliste, R. Caracas, M. Côté *et al.*, Comput. Phys. Commun. **180**, 2582 (2009).
[14] X. Gonze, F. Jollet, F. A. Araujo, D. Adams, B. Amadon, T. Applencourt, C. Audouze, J.-M. Beuken, J. Bieder, A. Bokhanchuk *et al.*, Comput. Phys. Commun. (to be published) (2016).
[15] R. M. Nieminen, E. Boroński, and L. J. Lantto, Phys. Rev. B **32**, 1377 (1985).
[16] E. Boroński and R. M. Nieminen, Phys. Rev. B **34**, 3820 (1986).
[17] P. E. Blöchl, Phys. Rev. B **50**, 17953 (1994).
[18] G. Kresse and D. Joubert, Phys. Rev. B **59**, 1758 (1999).
[19] N. A. W. Holzwarth, A. R. Tackett, and G. E. Matthews, Comput. Phys. Commun. **135**, 329 (2001).
[20] M. Torrent, F. Jollet, F. Bottin, G. Zérah, and X. Gonze, Comput. Mater. Sci. **42**, 337 (2008).
[21] M. Alatalo, B. Barbiellini, M. Hakala, H. Kauppinen, T. Korhonen, M. J. Puska, K. Saarinen, P. Hautojärvi, and R. M. Nieminen, Phys. Rev. B **54**, 2397 (1996).
[22] B. Barbiellini, M. Hakala, M. J. Puska, R. M. Nieminen, and A. A. Manuel, Phys. Rev. B **56**, 7136 (1997).
[23] I. Makkonen, M. Hakala, and M. J. Puska, Phys. Rev. B **73**, 035103 (2006).
[24] J. Arponen and E. Pajanne, J. Phys. F **9**, 2359 (1979).
[25] M. J. Puska, A. P. Seitsonen, and R. M. Nieminen, Phys. Rev. B **52**, 10947 (1995).
[26] H. Stachowiak and J. Lach, Phys. Rev. B **48**, 9828 (1993).
[27] N. D. Drummond, P. Lopez Ríos, R. J. Needs, and C. J. Pickard, Phys. Rev. Lett. **107**, 207402 (2011).
[28] B. Barbiellini, M. J. Puska, T. Korhonen, A. Harju, T. Torsti, and R. M. Nieminen, Phys. Rev. B **53**, 16201 (1996).
[29] B. Barbiellini, M. J. Puska, T. Torsti, and R. M. Nieminen, Phys. Rev. B **51**, 7341 (1995).
[30] J. Kuriplach and B. Barbiellini, Phys. Rev. B **89**, 155111 (2014).
[31] J. Kuriplach and B. Barbiellini, J. Phys.: Conf. Ser. **505**, 012040 (2014).
[32] B. Barbiellini and J. Kuriplach, Phys. Rev. Lett. **114**, 147401 (2015).
[33] F. Bruneval, J.-P. Crocombette, X. Gonze, B. Dorado, M. Torrent, and F. Jollet, Phys. Rev. B **89**, 045116 (2014).
[34] T. Korhonen, M. J. Puska, and R. M. Nieminen, Phys. Rev. B **54**, 15016 (1996).
[35] A. A. Rempel, W. Sprengel, K. Blaurock, K. J. Reichle, J. Major, and H.-E. Schaefer, Phys. Rev. Lett. **89**, 185501 (2002).
[36] A. Kawasuso, M. Yoshikawa, H. Itoh, R. Krause-Rehberg, F. Redmann, T. Higuchi, and K. Betsuyaku, Physica B **376**, 350 (2006).
[37] B. Barbiellini, J. Kuriplach, W. Anwand, and G. Brauer, in *MRS Proceedings* (Cambridge University, Cambridge, UK, 2000), Vol. 640, pp. H5–25.
[38] F. Linez, Ph.D. thesis, Université d'Orléans, 2012.